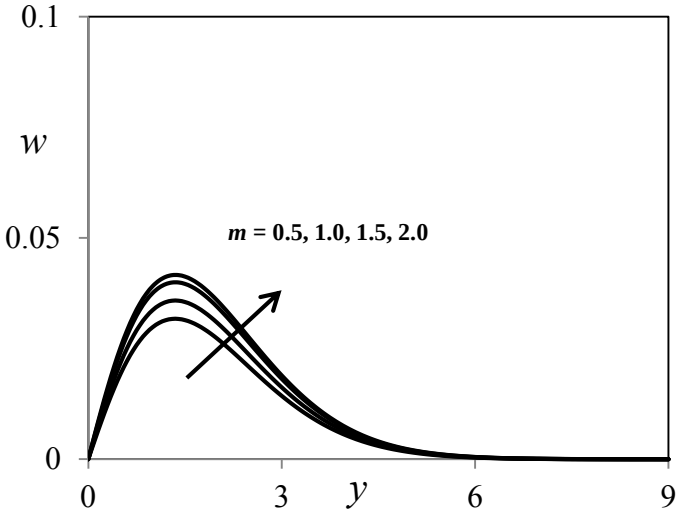

Fig. 16. Effect of *m* on *w*

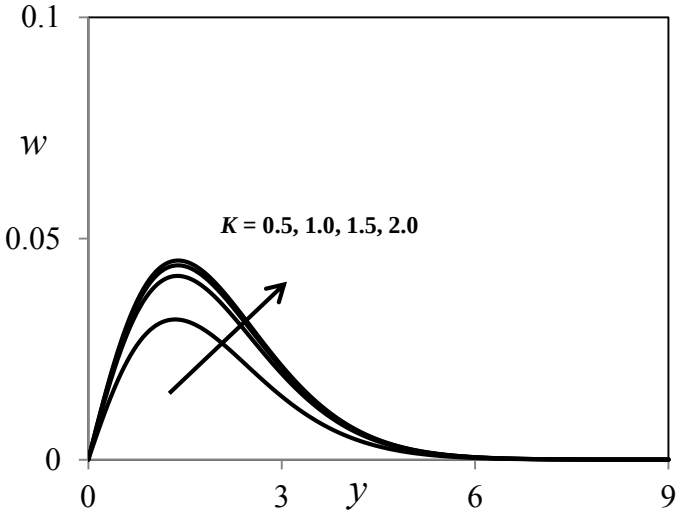

Fig. 17. Effect of *K* on *w*

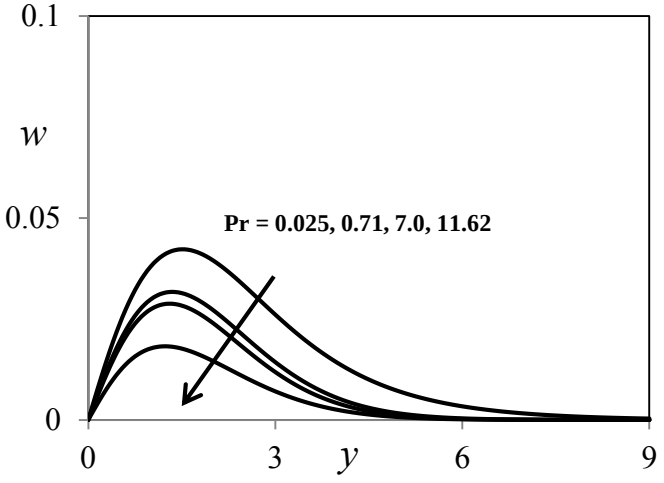

Fig. 18. Effect of Pr on *w*

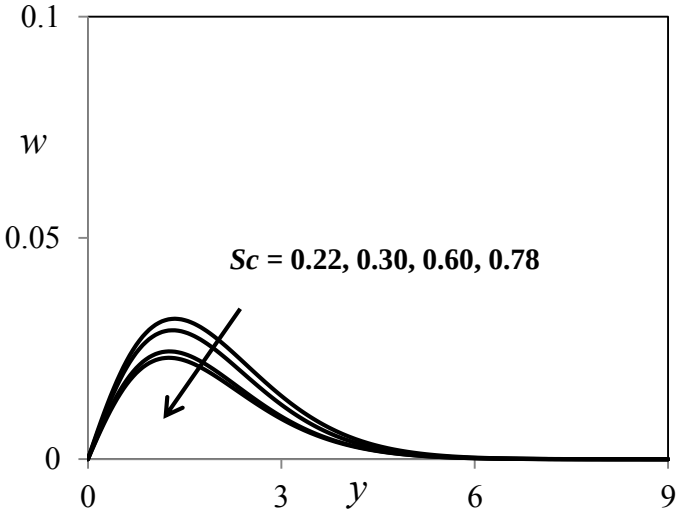

Fig. 19. Effect of *Sc* on *w*

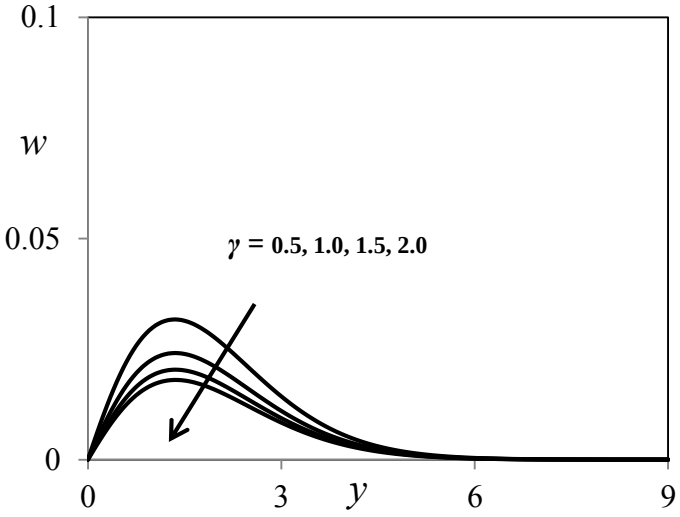

Fig. 20. Effect of *γ* on *w*

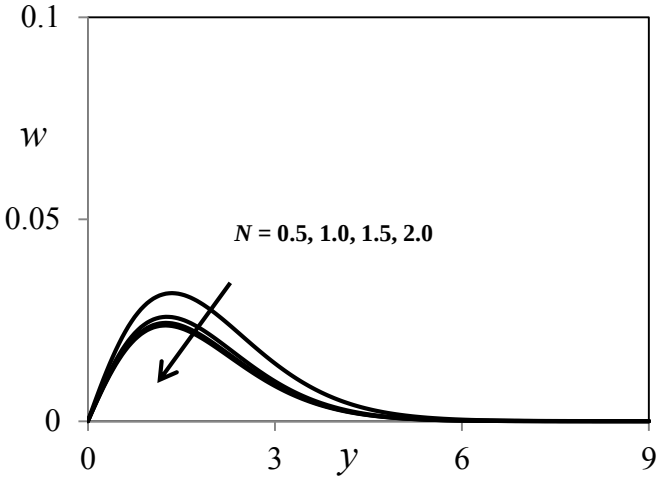

Fig. 21. Effect of *N* on *w*

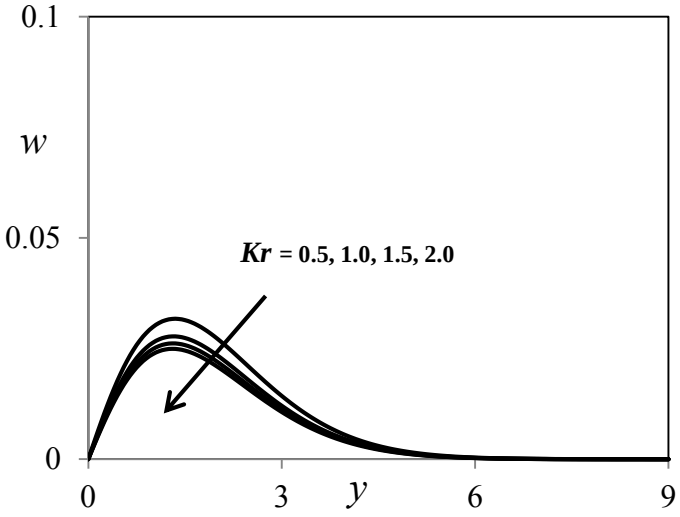

Fig. 22. Effect of *Kr* on *w*

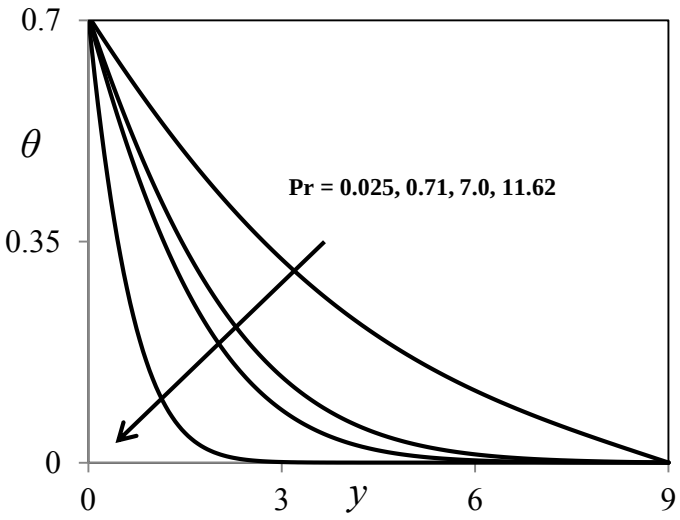

Fig. 23. Effect of Pr on θ

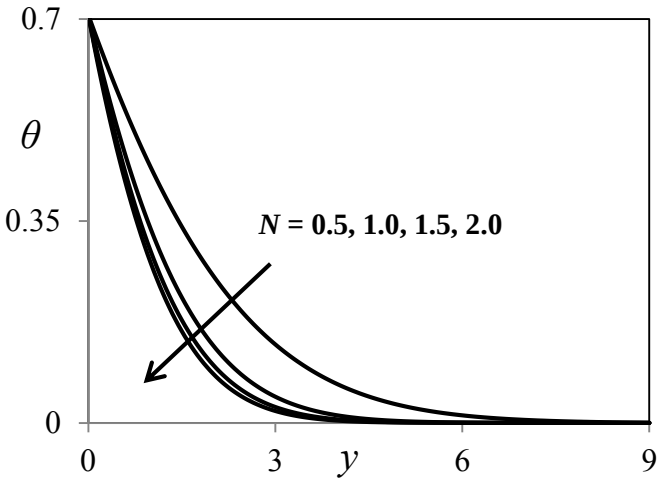

Fig. 24. Effect of *N* on θ

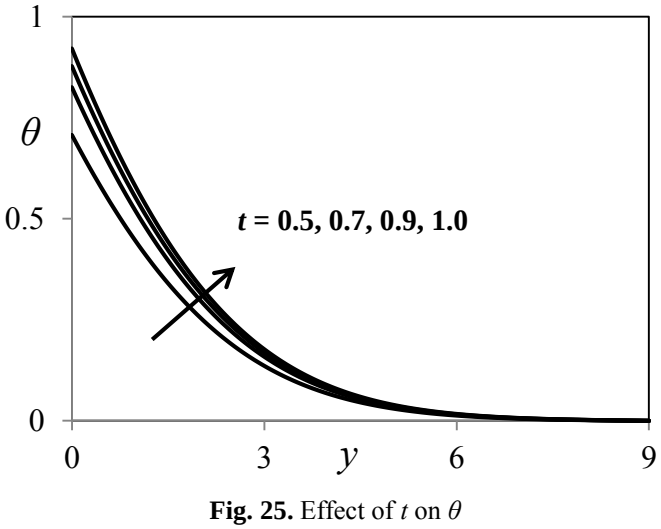

Fig. 25. Effect of *t* on θ

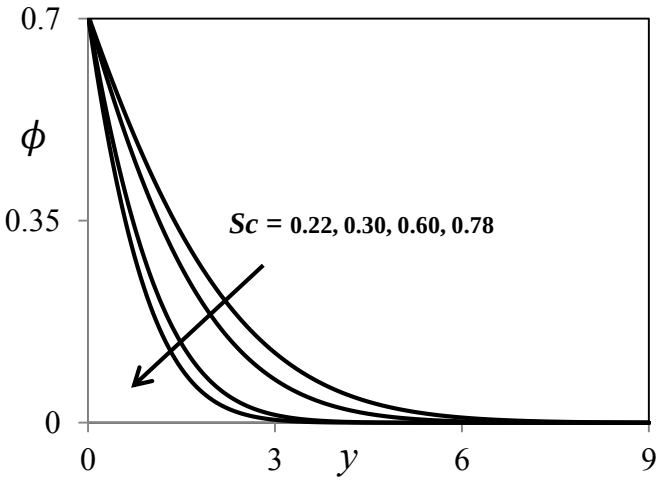

Fig. 26. Effect of *Sc* on ϕ

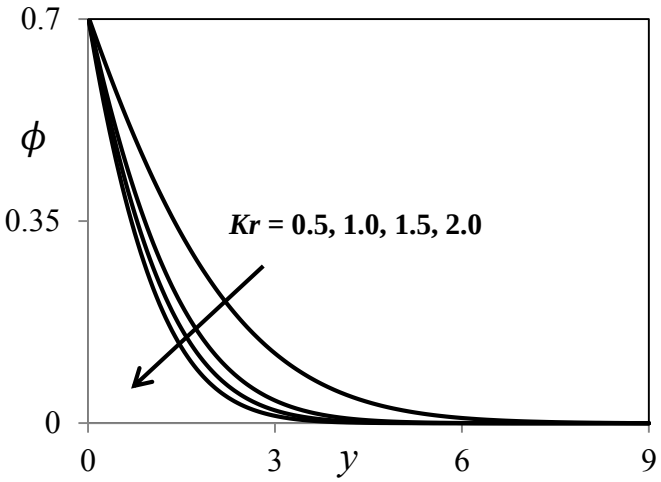

Fig. 27. Effect of *Kr* on ϕ

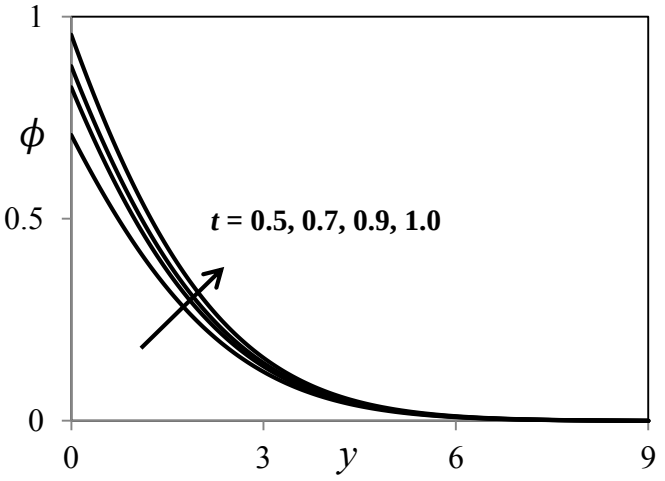

Fig. 28. Effect of t on ϕ

The equations (30), (31), (32) and (33) are similar and solved numerically using the boundary conditions (34). A graphical representation of the numerical results is shown in Figs. (2) to (28) to show the effect of various numbers on the flow of the limit level. In this study, we examined the effects various material parameters like Grashof number for heat transfer, Grashof number for mass transfer, Magnetic field parameter, Hall parameter, Permeability parameter, Prandtl number, Schmidt number, Casson fluid parameter, Angle of inclination parameter and Thermal radiation parameter to determine their respective effects clearly observe the velocity, temperature and concentration distributions of the flow. The numerical results of the skin-friction coefficient, rate of heat and mass transfer coefficients expressed in terms of Nusselt numbers or Sherwood numbers, are presented in tabular forms. The primary velocity, secondary velocity, temperature and concentration of the numerical calculation, the selected value of the horizontal Prandtl (Pr = 0.025), the air is 25^o *C* And atmospheric pressure (Pr = 0.71), water (Pr = 7.00) and water at 4^o*C*(Pr = 11.40).In order to draw attention to the value of the results obtained in the study, the values of *Sc*are hydrogen (*Sc*= 0.22), helium (*Sc*= 0.30), water vapour (*Sc*= 0.60) and ammonia (*Sc*= 0.78).For the physical meaning, the numerical discussion is in question and in $t = 1.0, \omega t = \pi/2$ to obtain stable values for velocity, temperature and concentration fields. To find a solution to this problem, a finite vertical infinite plate was placed in the flow. This solves the entire limited problem. However, in the picture, y values range from 0 to 9. Velocity, temperature and concentration tend to zero at $y_{max} = 9$. They tend to be 9.This is true for every value y, this study considers a finite length. The temperature and concentration of the material are coupled at primary velocity by the Grashof number of heat transfer, and the Grashof number of mass transfer is shown in equation (30).The effects of Grashof numbers for heat and mass transfer on primary velocity profiles are shown in Figs. 2 and 3 respectively. Grashof number for heat transfer number refers to the relative influence of thermal buoyancy on the dynamics of the viscous fluid in the boundary layer. As expected, an increase in primary velocity was observed due to an increase in thermal force. If *Gr* increased, the peak velocity of the primary velocity near the perforated plate increases rapidly and then descends smoothly at the velocity of free flow. The Grashof number of mass transfer determines the relationship between the buoyancy of the species and the dynamics of the viscous fluid. As expected, as the buoyancy of the species increases, the primary velocity of the fluid increases and the peak becomes more pronounced. The primary velocity profile reaches a significant maximum near the plate and is therefore appropriately reduced to approximate the value of the free flow. It should be noted that the primary velocity increases as the value of the Grashof mass transfer increases. Figs. 4 and 15 show the effect of the magnetic field parameter on primary and secondary velocities. As can be seen from these figures, with the increase of *M*, both the primary and the secondary velocities decrease. That is, the primary or secondary fluid is delayed due to the application of a transverse magnetic field. This phenomenon is clearly consistent with the fact that the Lorentz force due to the interaction of the magnetic field and the fluid velocity is subject to fluid movement. Fig. 12 shows the behaviour of the primary velocity distribution of various chemical reaction parameters *Kr*. *Kr* > 0 corresponding to a destructive chemical reaction. As can be seen from the profile, the primary velocity is reduced in the degraded chemical reaction in the boundary layer. This is because of the increase The rate of chemical reaction rate causes the pulses in the boundary layer to weaken in the degraded chemical reaction. The effects of Grashof number for heat and mass transfer numbers on the distribution of the secondary velocity are shown in Figs. 13 and 14. With increasing heat and mass transfer, this secondary velocity component also increases. In Fig. 27, as the concentration of the chemical reaction increases, the concentration decreases. The demonstration of a destructive chemical reaction indicates that the diffusion rate can be significantly modified by chemical reactions. This is because the chemical reaction has increased , it causes the concentration of the boundary layer to become thinner, thus reducing the concentration of the diffusive substance. This reduction in the concentration of the diffuser material reduces the mass diffusion. The effect of the Hall parameter *m* on the primary and secondary velocity profiles is shown in Figs. 5 and 16. We can see from these figures, the primary and secondary velocities increases Hall parameter increases. This is because the Hall current usually reduces the strength of the Lorentz force. This means that the Hall current tends to increase the fluid velocity component. Fig. 22 shows the effect of the chemical reaction parameters on the secondary velocity. It can be seen that as the value of this parameter increases, the secondary velocity profiles decreases. Fig. 23 shows the relationship between the temperature curve and y using different values of the number Prandtl (Pr).This number indicates that the temperature profile decreases as Prandtl number increases. This is because the fluid is highly conductive to the small values of the Prandtl number. Physically, as the Prandtl number increases, thermal diffusivity decreases and this phenomenon leads to a decrease in energy transfer capacity, which reduces the thermal interface.

Fig. 26 shows the concentration of various gases on the y curves, such as hydrogen (*Sc* = 0.22), helium (*Sc* = 0.30), water vapour (*Sc* = 0.60) and ammonia (*Sc* = 0.78).It has been

reported that the effect of increasing the Schmitt number (*Sc*) reduces the concentration of the concentration. This is consistent with the fact that the increase in *Sc* means a decrease in molecular diffusivity (*D*), which leads to a decrease in the concentration boundary layer. Therefore, for smaller *Sc* values, the concentration of the substance is greater and, for larger *Sc* values, the concentration of the substance is lower. Furthermore, it has been observed that the thickness of the concentration boundary layer has increased significantly with increasing frequency near the border, but the opposite tendency has been detected far from the plate. The influence of Schmidt number (*Sc*) on the primary and secondary velocities is shown in Figs. 8 and 19 respectively. From these figures, primary and secondary velocities decrease as Schmidt number increases. The Schmidt number represents the relationship between the moment and the mass diffusion coefficients. Schmidt's number then quantifies the relative validity of the momentum and mass transfer through the diffusion in the boundary layers of fluid dynamics (velocity) and concentration (species). The curves in Figs. 6 and 17 show the effect of the Permeability parameter (*K*) on primary and secondary velocities. As shown in Figs. 6 and 17, with this Permeability parameter increases, both the velocities in x' and z' directions increase. Figs. 11, 21 and 24 show an effect of thermal radiation (*N*) on the primary velocity, the secondary fluid temperature and the fluid velocity. From these figures, the thermal radiation of the door is reduced at each velocity and temperature. Physically, thermal radiation causes a decrease in the temperature of the fluid medium and, therefore, a decrease in the kinetic energy of the fluid particles. This results in a corresponding decrease in fluid velocity. Therefore, the Figs. 11, 21 and 24 are in good agreement with the laws of physics. So with the increase of *N, θ, u* and *w* will be reduced. Now, from these figures it can be inferred that the effect of radiation on temperature is greater than the effect on velocity. Therefore, thermal radiation does not have a significant effect on velocity, but it has a relatively more pronounced effect on the temperature of the mixture. Figs.25 and 28 show the effect of the time on temperature and concentration profiles. It is obvious from Figs. 25 and 28 where θ and ϕ increase as *t* increases. This means that the temperature and concentration of the fluid accelerates as time develops in the boundary layer region. The effect of Casson parameter (γ) on the profiles of fluid velocity in x'-direction (primary velocity) and z'-directions (secondary velocity) are shown graphically in Figs. 9 and 20 respectively. It is evident from these figures that on increasing the values of both Casson parameter, the fluid flow velocities (primary velocity and secondary velocity) decreases within the boundary layer region. The Casson parameter measures the yield stress and when it becomes large, the fluid behaves as a Newtonian fluid. The increase in the yield stress causes a stabilization effect. The effect of angle of inclination to the vertical direction on the velocity is shown in Fig. 10. From this figure we observe that the velocity is decreased by increasing the angle of inclination due to the fact that as the angle of inclination increases the effect of the buoyancy force due to thermal diffusion decreases by a factor of $\cos\alpha$. Consequently, the driving force to the fluid decreases as a result there is decrease in the velocity profile. From Figs. 7 and 18, we observe that as Pr increases, primary velocity profiles and secondary velocity profiles decrease respectively. This happens because when Pr increases the thermal boundary layer thickness rapidly decreases. This causes an increase in fluid viscosity. Consequently the primary velocity profiles and secondary velocity profiles decrease.

The influence of *Gr*,*Gc*,*M*,*m*,*K*, Pr,*Sc*,α, γ, *N* and *Kr* on skin-friction coefficient (Cf_1) due to primary velocity profiles is discussed in tables 1 and 2. From these tables, we observed that the skin-friction coefficient is increasing with increasing values of *Gr*,*Gc*,*m*,*K* and the reverse effect is observed with increasing of *M*, Pr,*Sc*,α, γ, *N*, *Kr*. The influence of *Gr*,*Gc*,*M*,*m*,*K*, Pr,*Sc*,α, γ, *N* and *Kr* on skin-friction coefficient (Cf_2) due to secondary velocity profiles is discussed in tables 1 and 3. From these tables, we observed that the secondary velocity skin-friction coefficient is rising with increasing values of *Gr*,*Gc*,*M*, *m*,*K* and the reverse effect is observed with increasing of Pr, *Sc*,α, γ, *N*, *Kr*. The influence of Pr , *N* and *t* on rate of heat transfer coefficient (*Nu*) due to temperature profiles is discussed in table 4. From this table, we observed that

the rate of heat transfer coefficient is increasing with increasing values of *t* and decreasing with increasing values of Pr and *N*. The influence of *Sc*, *Kr* and *t* on rate of mass transfer coefficient or Sherwood number (*Sh*) due to concentration profiles is discussed in table 5. From this table, we observed that the rate of mass transfer coefficient is increasing with increasing values of *t* decreasing with increasing values of *Sc* and *Kr*.

Table-1.: Numerical values of Skin-friction coefficients (Cf_1) due to primary velocity profiles and (Cf_2) due to secondary velocity profiles for different values of *Gr*, *Gc*, *M*, *K* and *m*

Gr	*Gc*	*M*	*K*	*m*	Cf_1	Cf_2
2.0	2.0	0.5	0.5	0.5	1.2558412458	0.4512235698
4.0	2.0	0.5	0.5	0.5	1.4522018478	0.6652148921
2.0	4.0	0.5	0.5	0.5	1.5011248201	0.7884120155
2.0	2.0	1.0	0.5	0.5	1.1544833927	0.5582215486
2.0	2.0	0.5	1.0	0.5	1.3224619485	0.5214662489
2.0	2.0	0.5	0.5	1.0	1.3222160991	0.5211630188

Table-2.: Numerical values of Skin-friction coefficient (Cf_1) due to primary velocity profiles for different values of γ, α, Pr, N, Sc and Kr

γ	α	Pr	N	Sc	Kr	Cf_1
0.5	45°	0.71	0.5	0.22	0.5	1.2558412458
1.0	45°	0.71	0.5	0.22	0.5	1.1885021349
0.5	90°	0.71	0.5	0.22	0.5	1.1799632045
0.5	45°	7.00	0.5	0.22	0.5	1.1055632478
0.5	45°	0.71	1.0	0.22	0.5	1.1662450124
0.5	45°	0.71	0.5	0.30	0.5	1.1553620188
0.5	45°	0.71	0.5	0.22	1.0	1.1662004875

Table-3.: Numerical values of Skin-friction coefficient (Cf_2) due to secondary velocity profiles for different values of γ, Pr, N, Sc and Kr

γ	Pr	N	Sc	Kr	Cf_2
0.5	0.71	0.5	0.22	0.5	0.4512235698
1.0	0.71	0.5	0.22	0.5	0.3884122478
0.5	7.00	0.5	0.22	0.5	0.3011466947
0.5	0.71	1.0	0.22	0.5	0.3441501486
0.5	0.71	0.5	0.30	0.5	0.3221688412
0.5	0.71	0.5	0.22	1.0	0.3622854719

Table-4.: Numerical values of rate of heat transfer coefficient (Nu) due to temperature profiles for different values of Pr, N and t

Pr	N	t	Nu
0.71	0.5	1.0	0.1544851256
7.00	0.5	1.0	0.0522148795
0.71	1.0	1.0	0.0877412516
0.71	0.5	2.0	0.2056221895

Table-5.: Numerical values of rate of mass transfer coefficient (Sh) due to concentration profiles for different values of Sc, Kr and t

Sc	Kr	t	Cf_2
0.22	0.5	1.0	0.1448522189
0.30	0.5	1.0	0.0755213369
0.22	1.0	1.0	0.0999521487
0.22	0.5	2.0	01999850125

1. Validation of Numerical Results:

To assess the correctness of the current finite difference method, the authors compared the results with published mass transfer rate data to understand the magnetohydrodynamic viscosity, the case where the incompressible fluid passes through the vertical porous plate and the porous plate exists in the porous medium. The hall current is calculated according to Sharma and Chaudhary of case [28] In the absence of Casson fluid, Angle of inclination, Thermal radiation and Chemical reactions, using different Schmidt values and phase angles, recorded other parameters. These results are all in table 6 shows these favourable comparisons show that the genius of numerical methods. Therefore, it is possible to use the code developed with great security to verify the problems involved in this document.

Table-6.: Sh is the Rate of mass transfer (Sherwood number) results obtained in the present study, and $C(t)$ is the rate of mass transfer results obtained by Sharma and Chaudhary[28].

	$C(t)$ (Analytical results of Sharma and Chaudhary[28])			Sh (Present Numerical results)		
$\omega \downarrow$	$Sc \rightarrow$	0.22	0.30	0.78	0.22	0.30	0.78
0.0		0.2200	0.3000	0.7800	0.2200000000	0.3000000000	0.7800000000
0.2		0.0800	0.1200	0.3800	0.0800124458	0.1200541846	0.3799995824
0.4		- 0.1700	- 0.2100	- 0.4100	- 0.1742122215	- 0.2055124551	- 0.4001251655
0.6		- 0.2700	- 0.3500	- 0.8100	- 0.2622154855	- 0.34112051894	- 0.8001452188
0.8		- 0.0800	- 0.1200	0.3900	- 0.0801145232	- 0.12022101577	0.3899952734
1.0		0.2100	0.2600	0.4400	0.2100154825	0.2511862015	0.4388521492

2. Conclusions:

This work investigated the effect of a chemical reaction and thermal radiation on magneto hydrodynamics mixed convection through a vertically inclined perforated plate immersed in a porous medium with Hall current, heat and mass transfer. The linear coupled partial differential equation obtained is solved using the finite difference method. The authors studied a parametric study, illustrates the impact of different traffic parameters of velocity, temperature and concentration fields. The shear stress on the plate due to the primary and secondary velocity fields and the heat transfer and the mass transfer coefficients due to temperature and concentration are obtained in a dimensionless form. The results are displayed in graphical and tabular form. The authors concluded that the flow field and physical interest are significantly influenced by these parameters.

i. Because of the Lorentz magnetic force acting on the flow field, the action of the transverse magnetic field decreases the primary and secondary motions, which are accelerated by the Hall effect.

ii. The movement of the liquid is delayed due to chemical reactions. Therefore, the consumption of chemicals leads to a decrease in the concentration field, which in turn The buoyancy effect due to the concentration gradient is reduced. Therefore, the flow field is delayed.

iii. The concentration of the fluid is reduced due to the chemical reaction. This is due to the chemical consumption decreased range of concentrations of species.

iv. The Grashof number, which increases heat and mass transfer, has been found to improve the effects of thermal buoyancy and concentration, thus increasing primary and secondary velocities.

v. As the Schmidt number increases, the concentration distribution of the flow field decreases at all points. This means that the most common substances have a greater delay in the distribution of the concentration of the flow field.

vi. The Prandtl number reduces the flow field temperature at all points. The higher the Prandtl number, the sharper the flow field temperature decreases.

vii. The results obtained for the specific case of the problem were compared with the documents previously published and found in good agreement

3. Nomenclature:

List of variables:

$\overline{B}$ Magnetic Induction Vector

B_o Intensity of the applied magnetic field ($A\ m^{-1}$)

C' Dimensionless species concentration of the fluid

C_p Specific heat at constant pressure ($J\,Kg^{-1}K$)

C'_∞ Concentration in the fluid far away from the plate ($Kg\ m^{-3}$)

C'_w Concentration of the fluid at the wall ($Kg\ m^{-3}$)

D Chemical molecular diffusivity ($m^2\ s^{-1}$)

D_T Coefficient of chemical thermal diffusivity, $M^1L^{-1}T^{-1}K^{-1}$

$\overline{E}$ Electric field

e Electron charge, $Coloumb$

Gr Grashof number for heat transfer

Gc Grashof number for mass transfer

Pr Prandtl number

Sc Schmidt number

q_r Radiative heat flux

N Thermal radiation parameter

p_e Electron pressure ($N\ m^{-2}$)

Kr Chemical reaction parameter

T' Temperature of the fluid (K)

T'_w Temperature of the plate (K)

T'_∞ Fluid temperature far away from the plate (K)

t Time (s)

u Velocity component in $x'-$direction ($m\ s^{-1}$)

$\overline{V}$ Velocity vector

V_o Reference velocity ($m\ s^{-1}$)

w Velocity component in $z'-$direction ($m\ s^{-1}$)

g Acceleration due to gravity ($m\ s^{-2}$)

$\overline{J}$ Electric current density vector

K Permeability of the porous medium

M Hartmann number or Magnetic field parameter

m Hall parameter

Nu Rate of heat transfer coefficient (or) Nusselt number

Sh Rate of mass transfer coefficient (or) Sherwood number

Cf_1 Skin-friction due to velocity (u) (N/m^2)

Cf_2 Skin-friction due to velocity (w) (N/m^2)

Greek symbols:

β Coefficient of Volume expansion $\left(K^{-1}\right)$

ρ Density of the fluid $\left(kg/m^{-3}\right)$

β^* Volumetric Coefficient of expansion with Concentration($m^3\ Kg^{-1}$)

ν Kinematic Viscosity $\left(m^2 s^{-1}\right)$

ω_e Electron frequency (*Hertz*)

τ'_w Shear stress (N/m^2)

ωt Phase Angle (*radians*)

Ω Angular frequency (*Hertz*)

ω Frequency parameter

θ Dimensionless Temperature $\left(K\right)$

σ Electrical conductivity, ($\Omega^{-1}m^{-1}$)

τ_e Electron collision time (s)

τ_i Ion collision time (s)

n_e Number of electron density

ω_i Ion frequency (*Hertz*)

κ Thermal conductivity, W/mK

α Angle of inclination parameter (*degrees*)

γ Casson fluid parameter

Superscript:

$/$ Dimensionless properties

Subscripts:

w Conditions on the wall

∞ Free stream conditions

p Plate

REFERENCES

[1] H. Alfven, Existence of electromagnetic-hydrodynamic waves, Nature, 150 (1942), pp. 405-406.

[2] E. Hall, On a new action of the magnet on electric currents, Am J Math, 2 (1879), pp. 287-292

[3] I. Pop, V.M. Soundalgekar, Effects of Hall currents on hydrodynamic flow near a porous plate, Acta Mech, 20 (1974), pp. 315-318.

[4] S. Ahmed, J. Zueco Modeling of heat and mass transfer in a rotating vertical porous channel with hall current, Chem Eng Comm, 198 (2011), pp. 1294-1308.

[5] A.M. Aziz, Effects of hall current on the flow and heat transfer of a nanofluid over a stretching sheet with partial slip, Int J Mod Phys C, 24 (2013), p. 1350044.

[6] T. Hayat, M. Awais, M. Nawaz, S. Iram, A. Alsaedi, Mixed convection three-dimensional flow with Hall and ion-slip effects, Int J Nonlinear Sci Numer Simul, 14 (2013), pp. 167-177.

[7] P. Sulochana, Hall effects on unsteady MHD three dimensional flow through a porous medium in a rotating parallel plate channel with the effect of the inclined magnetic field, Am J Comput Math, 4 (2014), pp. 396-405.

[8] K. A. Yih, Free convection effect on MHD coupled heat and mass transfer of a moving permeable vertical surface, Int Commun Heat Mass Transfer, 26 (1999), pp. 95-104.

[9] M. A. Hossain, Effect of Hall current on unsteady hydromagnetic free convection flow near an infinite vertical porous plate, J Phys Soc Jpn, 55 (7) (1986), pp. 2183-2190.

[10] M. A. Hossain, K. Mahammad, Effect of Hall current on hydromagnetic free convection flow near an accelerated porous plate, Jpn J Appl Phys, 27 (8) (1988), pp. 1531-1535.

[11] A. M. Salem, M. Abd El-Aziz, Effect of Hall currents and chemical reaction on a hydromagnetic flow of a stretching vertical surface with internal heat generation/absorption, Appl Math Model, 32 (7) (2008), pp. 1236-1254.

[12] S. K. Ghosh, O. Anwar Bég, M. Narahari, Hall effects on MHD flow in a rotating system with heat transfer characteristics, Meccanica, 44 (2009), pp.

741-765.

[13] M. Abd El-Aziz, Flow and heat transfer over an unsteady stretching surface with Hall effect, Meccanica, 45 (2010), pp. 97-109.

[14] R. D. Cess, The interaction of thermal radiation with free convection heat transfer, Int J Heat Mass Transfer, 9 (1966), pp. 1269-1277.

[15] V. S. Arpaci, Effect of thermal radiation on the laminar free convection from a heated vertical plate, Int J Heat Mass Transfer, 11 (1968), pp. 871-881.

[16] M. Gnaneswara Reddy, N. Bhaskar Reddy, Radiation and mass transfer effects on unsteady MHD free convection flow past a vertical porous plate with viscous dissipation, Int J Appl Math Mech, 6 (6) (2010), pp. 96-110.

[17] M. Gnaneswara Reddy, N. Bhaskar Reddy, Mass transfer and heat generation effects on MHD free convection flow past an inclined vertical surface in a porous medium, J Appl Fluid Mech, 4 (3) (2011), pp. 7-11

[18] A. Basiri Parsa, M. M. Rashidi, T. Hayat, MHD boundary-layer flow over a stretching surface with internal heat generation or absorption, Heat Trans-Asian Res, 42 (6), 500-514, 2013.

[19] M. Gnaneswara Reddy, Effects of thermophoresis, viscous dissipation and joule heating on steady MHD heat and mass transfer flow over an inclined radiative isothermal permeable surface with variable thermal conductivity, Int J Heat Technol, 30 (1) (2012), pp. 99-110.

[20] M. A. Hossain, M. A. Alim, D. A. Rees, The effect of radiation on free convection from a porous vertical plate, Int. J. Heat Mass Transfer, 42 (1999), pp. 181-191.

[21] M. A. Hossain, H. S. Takhar, Radiation effect on mixed convection along a vertical plate with uniform surface temperature, Int. J. Heat Mass Transfer, 31 (1996), pp. 243-248.

[22] Dulal Pal, M. S. Malashetty, Radiation effects on stagnation-point flow over a stretching sheet with internal heat generation or absorption, Int. J. Appl. Mech. Eng., 13 (2008), pp. 427-439.

[23] S. Mukhopadhyay, G. C. Layek, Effects of thermal radiation and variable fluid viscosity on free convective flow and heat transfer past a porous stretching surface, Int. J. Heat Mass Transfer, 51 (2008), pp. 2167-2178.

[24] Dulal Pal, Heat and mass transfer in stagnation-point flow towards a stretching surface in the presence of buoyancy force and thermal radiation, Meccanica, 44 (2009), pp. 145-158.

[25] S. Shateyi, S. S. Motsa, Thermal radiation effects on heat and mass transfer over an unsteady stretching surface, Math. Probl. Eng., 2009 (2009), Article ID 965603, 13 pages.

[26] Y. Khan, Q. Wu, N. Faraz, A. Yildirim, S. T. Mohyud-Din, Heat transfer analysis on the magnetohydrodynamic flow of a non-Newtonian fluid in the presence of thermal radiation: an analytic solution, Z. Nat.forsch. A, 67a (2012), pp. 147-152.

[27] Md. Madani, Y. Khan, M. Fathizadeh, A. Yildirim, Application of homotopy perturbation and numerical methods to the magneto-micropolar fluid flow in the presence of radiation, Eng. Comput., 29 (3) (2012), pp. 277-294.

[28] B. K. Sharma, R. C. Chaudhary, Hydromagnetic Unsteady Mixed Convection And Mass Transfer Flow Past A Vertical Porous Plate Immersed In A Porous Medium With Hall Effect, Eng. Trans., 56, 1, 3-23, 2008.

[29] P. Sturdza, An aerodynamic design method for supersonic natural laminar flow aircraft Ph. D. thesis. California, USA: Dept. Aeronautics and Astronautics, Stanford University; 2003.

[30] Sparrow EM, Cess RD. Radiation heat transfer. Belmont, Calif.: Brooks/Cole; 1966.